OPTICS AND SPECTROSCOPY

Protection against UWB pulses in hybrid quasi-reflectionless structures based on coupled lines and t-Resonators

I. A. Ivantsov · S. V. Vlasov · Y. S. Zhechev · R. S. Surovtsev

Received: 15 February 2026 / Revised: 7 April 2026 / Accepted: 6 May 2026
© The Author(s), under exclusive licence to Springer Nature Switzerland AG 2026

Abstract
This paper presents the experimental and numerical study of a hybrid electromagnetic protection device designed to suppress ultra-wideband (UWB) pulses. The device combines modal filtration and frequency-selective absorption based on T-resonators on broadside-coupled coplanar transmission lines. The proposed hybrid structure with two pairs of resonators attenuates the peak voltage by 4.2 times of UWB pulses with a 300 ps rise time and Gaussian pulses by 7.15 times, while maintaining the quasi-reflectionless behavior and supporting the data transmission rate up to 250 Mbps. The paper confirms the effectiveness of combining the modal dispersion with resonant structures to improve the electromagnetic compatibility without a significant signal degradation.

Keywords Electromagnetic compatibility · Ultra-wideband pulse · Modal filtration · Modal decomposition · Broadside-coupled coplanar transmission line · T-resonator · Quasi-reflectionless protection · Signal integrity

Introduction

The electromagnetic compatibility of radio-electronic systems remains a fundamental challenge in modern science and engineering [1–3]. The protection of sensitive equipment against ultra-wideband (UWB) electromagnetic pulses of nanosecond and sub-nanosecond durations is a critical issue. Due to their broad spectral content, such pulses can penetrate shielding and propagate along conductive paths, disrupting the operation of high-speed digital interfaces [4–6].

Conventional protection methods often rely on reflective filters, e.g., lumped L and C elements. While effective in the frequency domain, these devices usually demonstrate high reflection coefficients in the stopband. This leads to the reflection of the interference energy back toward the source or other parts of the system, potentially causing secondary malfunctions or standing waves. Consequently, there is a growing interest in quasi-reflectionless or absorption protection devices integrated into a printed circuit board [7, 8].

Modal filtration is a promising approach to the implementation of such devices [9–11]. Physical principle of modal filtration are based on the modal dispersion in coupled transmission lines with inhomogeneous dielectric filling. When a pulse enters the coupled section, it excites multiple propagation modes (typically even and odd) that propagate with different phase velocities. This difference induces an input pulse decomposition into a sequence of pulses with lower amplitudes at the output. Since the energy redistributes in the time domain and partially dissipates in matched terminations of the passive line, the device exhibits a low reflection coefficient over a wide frequency range.

However, physical dimensions of classical modal filters (MF) significantly reduces their application. In order to achieve a sufficient time separation of the modes, the coupled line must have a considerable length [12,

 https://doi.org/10.1007/s11182-026-03757-4

Published online: 25 September 2026

13]. Various approaches are proposed to enhance the modal decomposition efficiency while reducing physical dimensions. They include electromagnetic absorbers [14], reflection-symmetric structures [15], and hybrid combinations with TVS diodes [16], RLC-circuits [17], or UWB absorbers [18].

Microstrip resonators represent another class of integrated protection elements. While they act as stopband filters, their combination with modal filtration offers a unique mechanism for the pulse suppression. The integration of T-shaped resonators into an MF structure introduces additional signal paths. The interference wave reflection from the resonator ends with the main propagating modes can lead to a further pulse decomposition and attenuation [19, 20].

Zhechev and Zabolotsky [19] demonstrated that parametric optimization of quarter-wave resonators doubled the attenuation coefficient. In our recent research [20], we proposed an MF theoretical model with multiple T-resonators demonstrating a potential 13-fold reduction in the pulse amplitude. However, these studies were primarily theoretical and lacked the comprehensive experimental verification of the quasi-reflectionless property and signal integrity in real prototypes.

The aim of this work is to experimentally investigate the UWB pulse suppression capability of the hybrid protection device combining a modal filter with T-resonators. The full-wave electrodynamic analysis is performed for the structures, focusing on the time-domain decomposition of UWB pulses, the frequency-domain scattering parameters (the reflection loss in stopband filters), and preservation of the signal integrity for a high-speed data transmission.

Structure description and theoretical analysis

The cross-sectional views of the structures are shown in Fig. 1. The basic element is the MF formed by two broadside-coupled coplanar transmission lines locating on opposite sides of a dielectric substrate. The T-resonator is implemented as a coplanar line segment with a reference conductor.

Geometric parameters were chosen to provide a strong electromagnetic coupling between the lines with 1500 μm signal conductor width w_1, 500 μm ground gap s_1, and $5w_1$ total width d_1 of the ground plane. For the second line, $w_2 = 800$ μm, $s_2 = 500$ μm, and $d_2 = 5w_2$. The substrate material is FR-4 510 μm thick, and 35 μm copper thickness, 4.5 relative permittivity, and 0.018 loss tangent. Top and bottom ground planes are connected by a series *via* holes along signal traces to ensure the potential equalization and suppress parasitic parallel-plate modes. Figure 2 illustrates equivalent circuit models of the three prototypes. The low-pass filter (LPF) is a reference MF without resonators (LPF_1), LPF_2 is a hybrid structure with one pair of *T*-resonators, and LPF_3 is a hybrid structure with two pairs of *T*-resonators.

The circuits are symmetric to provide identical return loss characteristics for Ports 1 and 2. Resistors R_3 and R_4 (50 Ω) at the ends of the passive line are critical for the quasi-reflectionless operation. They dissipate the energy of decomposed modes, preventing reflection back to the input port.

The operation principle is based on the decomposition of the input UWB pulse with t_Σ duration into a sequence of pulses with lower amplitudes. In the coupled line section of length l_m, the pulse splits into modes propagating with different per-unit-length delays τ_{min} (fast mode) and τ_{max} (slow mode). The condition for a complete time-domain separation of modal pulses is given by

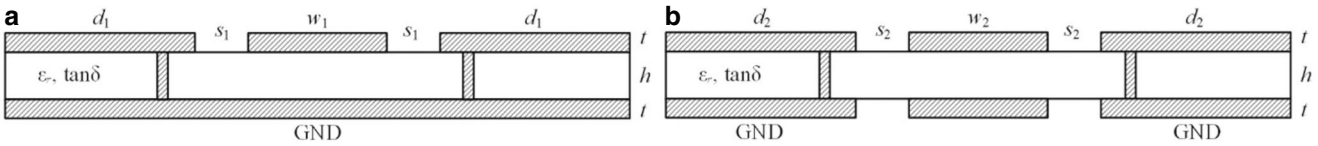


Fig. 1 Cross-sectional view of broadside-coupled coplanar transmission lines: **a** coplanar waveguide for the *T*-resonator, **b** transmission lines forming the MF

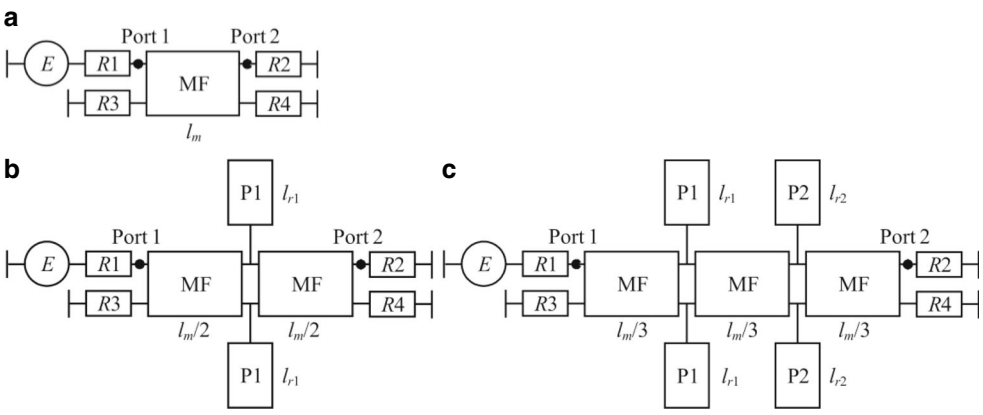


Fig. 2 Equivalent circuits of prototypes: **a** LPF_1 (reference MF); **b** LPF_2 (with one pair of *T*-resonators); **c** LPF3 (with two pairs of *T*-resonators). R_1 and R_2 are source/load impedances, R_3 and R_4 are matching terminations

$$t_{\sum} \leq (\tau_{max} - \tau_{\min}) \cdot l_{\mathrm{m}}. \tag{1}$$

When the condition (1) is met, two distinct pulses appear at the MF output. The integration of *T*-resonators introduces the additional multipath interference. A portion of the signal energy enters the resonator, reflects from its open end, and returns to the main line with a time delay determined by the resonator length.

In order to maximize the peak voltage suppression, resonator lengths (l_{r1} and l_{r2}) are synthesized such that the reflected pulses arrive at the output at time intervals between the main modal pulses, avoiding the superposition. The synthesis is performed using the following equations derived from the transmission line theory:

$$l_{r1} = l_{\mathrm{m}} \cdot (\tau_{\mathrm{m}max} - \tau_{\mathrm{m}\min}) / (4\tau_r), \tag{2}$$

$$l_{r2} = l_{\mathrm{m}} \cdot (\tau_{\mathrm{m}max} - \tau_{\mathrm{m}\min}) / \tau_r, \tag{3}$$

where τ_r is the per-unit-length delay of the fundamental mode in the *T*-resonator line.

Preliminary simulation was performed in the TUSUR.EMC computer simulation system [21]. The calculation was based on the method of moments, which allowed computing matrices of per-unit-length electrostatic induction (**C**) and electromagnetic inductance (**L**). The modal delay τ_i was obtained as square roots of eigenvalues of the matrix product $\mathbf{M} = \mathbf{LC}$.

Using Eqs. 1–3 and the calculated per-unit-length parameters, the best geometric length was determined, *viz.* $l_m = 500$ mm for the main line, $l_{r1} = 39$ mm for the first resonator pair, and $l_{r2} = 156$ mm for the second pair.

Experimental prototypes and measurement technique

Three experimental board prototypes were fabricated based on the calculated geometric parameters. Each board was 100×100 mm^2 in size, as shown in Fig. 3. SMA connectors for the surface mounting were installed at input and output Ports 1 and 2 for measurements. For the quasi-reflectionless operation, the ends of passive conductors were terminated with 50 Ω chip resistors (0804 package), which acted as matched loads for even and odd modes propagating in coupled lines.

The frequency characteristics of the prototypes were measured using a Panorama P4226 vector network analyzer (VNA). The block diagram and the photograph of the experimental setup are presented in Fig. 4. The setup included the VNA, the device under test (DUT), and a personal computer (PC) for the data acquisition and processing. Prior to measurements, a full two-port SOLT (Short-Open-Load-Thru) calibration was performed using the HKMM-13-13P calibration kit to eliminate systematic errors associated with the test setup, specifically those introduced by cables and adapters. The measurements were conducted in the frequency range from 10 MHz

https://doi.org/10.1007/s11182-026-03757-4

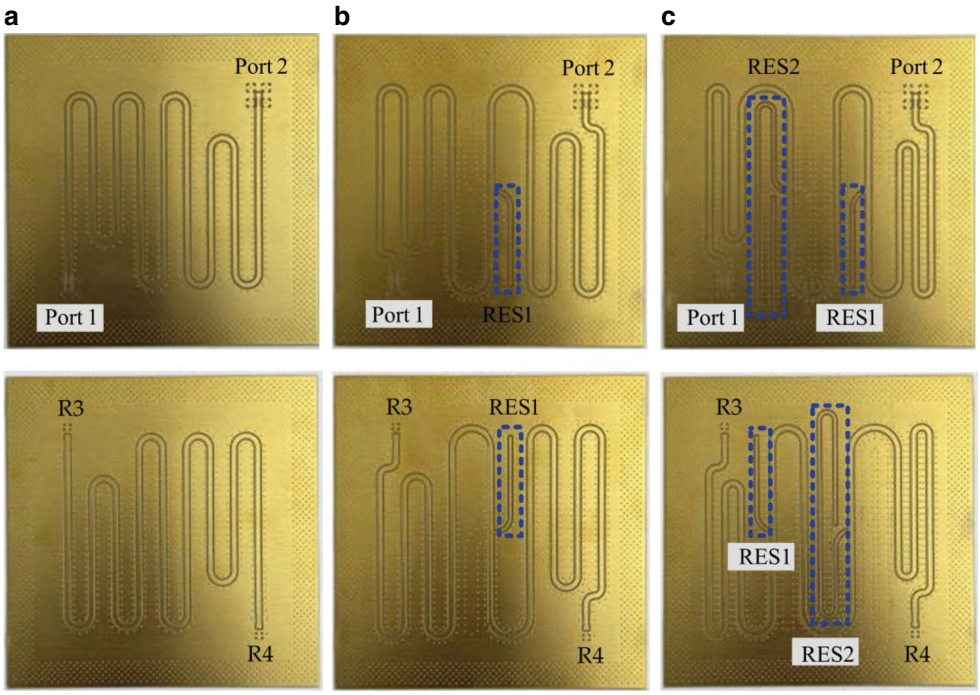


Fig. 3 Top and bottom views of the fabricated prototypes: **a** LPF_1, **b** LPF_2, **c** LPF_3

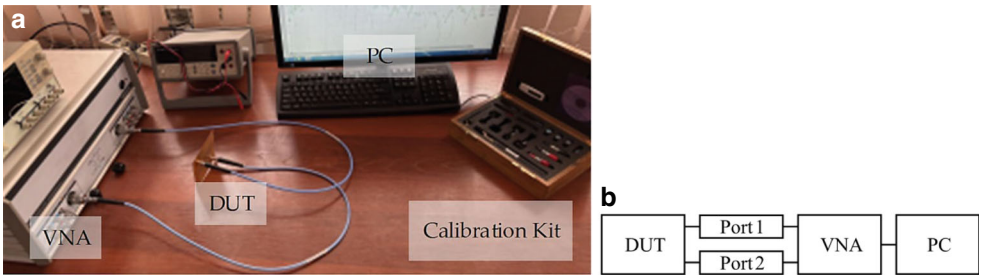


Fig. 4 Experimental setup for *S*-parameter measurements: **a** full view, **b** VNA, DUT, and PC connections

to 18 GHz. The upper frequency limit was determined by the operating range of the coaxial-to-microstrip transition. The measurement accuracy for the transmission coefficient magnitude was not over ±0.05 dB.

Frequency-domain analysis and validation

The measured and simulated frequency dependencies of scattering parameters (*S*-parameters) are presented in Fig. 5. The finite-difference time-domain (FDTD) method was used for full-wave simulation in the range of 0 to 20 GHz. For the reference structure (LPF_1), the transmission coefficient $|S_{21}|$ monotonically decreased with a characteristic comb-like pattern, typical for transversal filters based on coupled lines. The cut-off frequency (defined at a –3 dB level) was $f_c \approx 171$ MHz. The introduction of T-resonators (LPF_2 and LPF_3) modified the frequency response through a superposition of the modal interference and the resonance absorption of resonators.

The addition of resonators increased the suppression efficiency. The mean attenuation in the stopband (calculated up to 18 GHz) increased from 17.9 dB for LPF_1 to 21.6 dB for LPF_2 and 24.3 dB for LPF_3. This 6.4 dB increase corresponded to more than a two-fold reduction in the transmitted voltage amplitude averaged over the spectrum. In the passband, all prototypes demonstrated good matching with $|S_{11}|$ generally below –10 dB. In the stopband, the behavior was quasi-reflectionless. Unlike conventional reflective filters, where $|S_{11}| \to 0$ dB (total reflection), the proposed structures maintained relatively high return loss. Although local resonant peaks

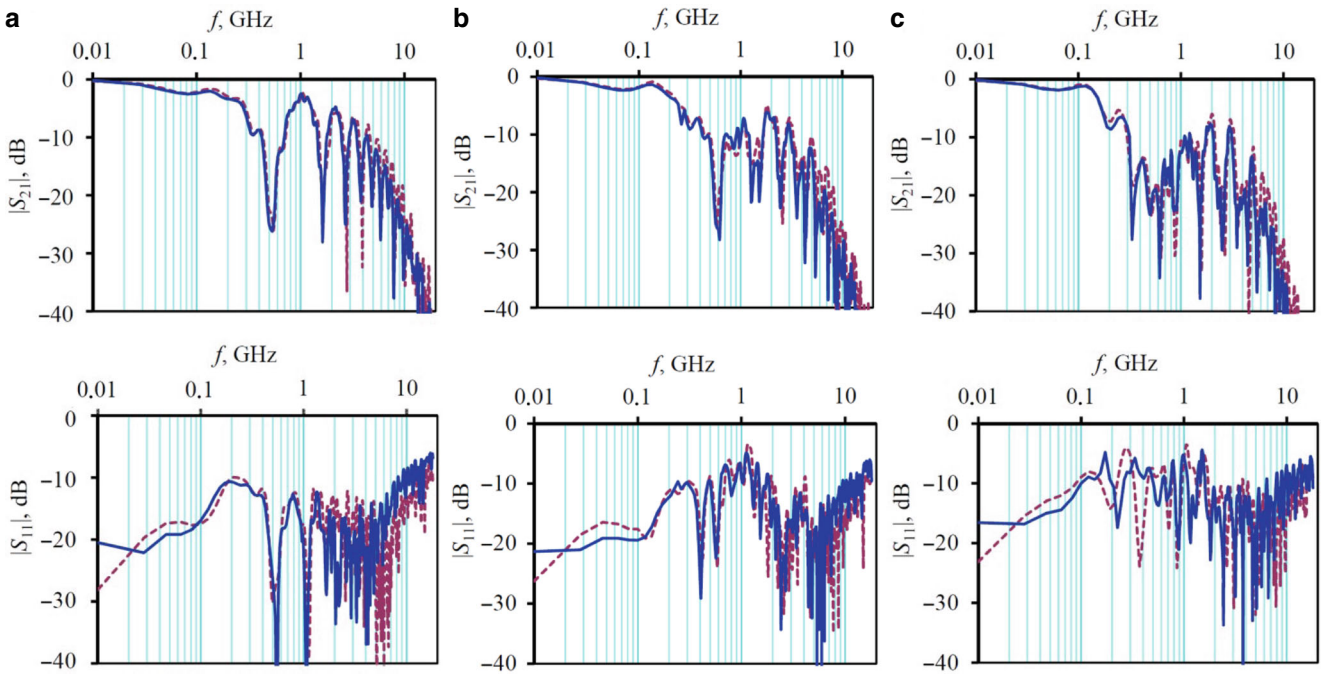


Fig. 5 Frequency dependences of *S*-parameters obtained by the FDTD simulation (dashed lines) and VNA measurements (solid lines): **a** LPF_1, **b** LPF_2, **c** LPF_3

of the reflection (up to –5 dB) were observed near the band edges (e.g., 0.5–2 GHz range for LPF_2 and LPF_3), the average return loss in the stopband remained at 10 to 12 dB. This confirmed that a significant portion of the stopband energy was dissipated in matching resistors R_3 and R_4, rather than reflected to the source.

Figures 6 and 7 illustrate the transmission coefficient and the group delay in the low (0–1 GHz) frequency range. While the group delay is a critical metric for the signal integrity primarily within the passband, its behavior in the transition and stopbands serves as an indicator of physical resonance phenomena. For LPF_1, the characteristics are linear and flat. For LPF_2 and LPF_3, strong nonlinearities and group delay peaks (reaching 8 to 10 ns) appear in the range of 300 to 600 MHz. These singularities correspond to the resonant frequency of T-resonators and destructive interference between the modes. The presence of these peaks confirms the dispersive mechanism required for the time-domain decomposition of pulses.

In order to quantify the agreement between the FDTD model and VNA measurements, the feature selective validation (FSV) method was employed [22]. The FSV analysis (see Fig. 8) decomposed the difference between datasets into amplitude and feature components. The resulting diagrams for $|S_{21}|$ showed a predominance of *Excellent* and *Very Good* ratings across the entire frequency range up to 18 GHz. Discrepancies observed in the

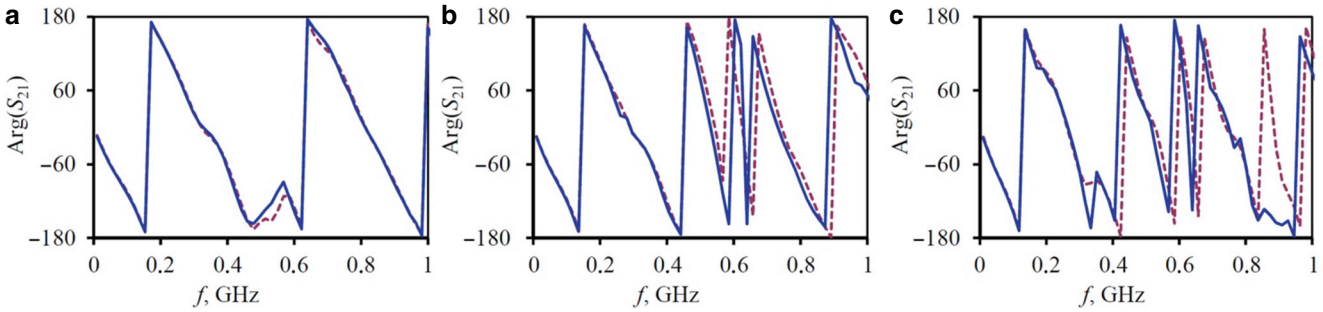


Fig. 6 S_{21} phases within 0–1 GHz obtained by FDTD simulation (dashed lines) and VNA measurements (solid lines): **a** LPF_1, **b** LPF_2, **c** LPF_3

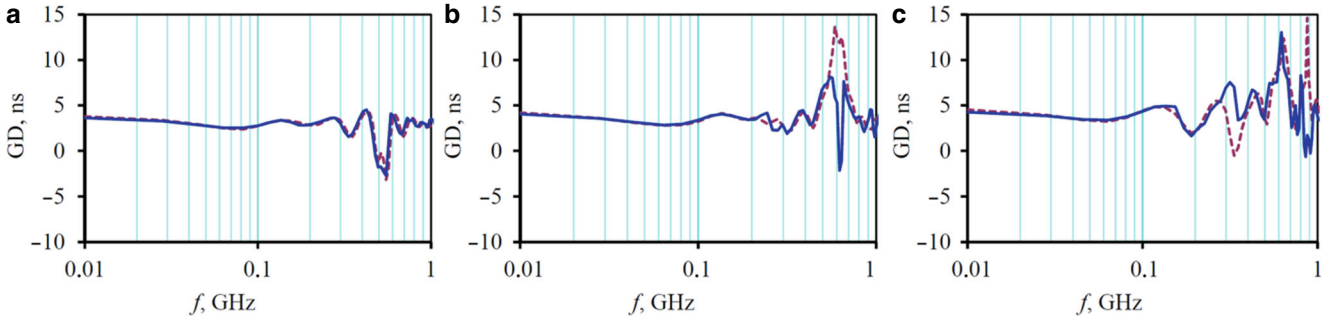


Fig. 7 Group delay within 0–1 GHz obtained by FDTD simulation (dashed lines) and VNA measurements (solid lines): **a** LPF_1, **b** LPF_2, **c** LPF_3

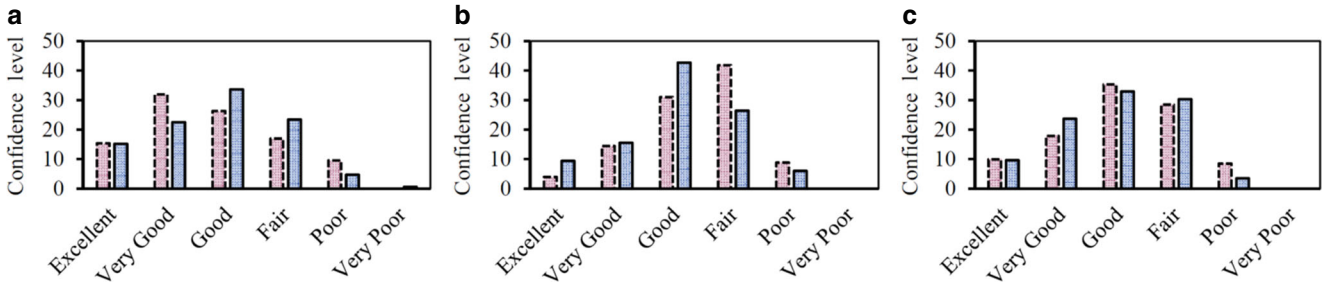


Fig. 8 FSV validation diagrams comparing simulated and measured $|S_{21}|$ up to 10 GHz (dashed lines) and 18 GHz (solid lines): **a** LPF_1, **b** LPF_2, **c** LPF_3

high-frequency region could be attributed to the manufacturing tolerance of the FR-4 substrate and parasitic effects of the SMA connector soldering, which were not fully captured in the numerical model.

Time-domain analysis

Based on the obtained *S*-parameters, the time-domain analysis was performed to evaluate the protection efficiency against the transient interference. The output voltage response $U_{out}(t)$ was calculated using the inverse fast Fourier transform of the product of the input signal spectrum $U_{in}(\omega)$ and the complex transmission coefficient $S_{21}(\omega)$. According to Fig. 9, two standard excitation signals were used such as the Gaussian pulse within 0.1–6 GHz, representing a generic wideband interference [23], and the UWB pulse with 1 V peak voltage and 300 ps duration at half-maximum, representing the intentional electromagnetic interference.

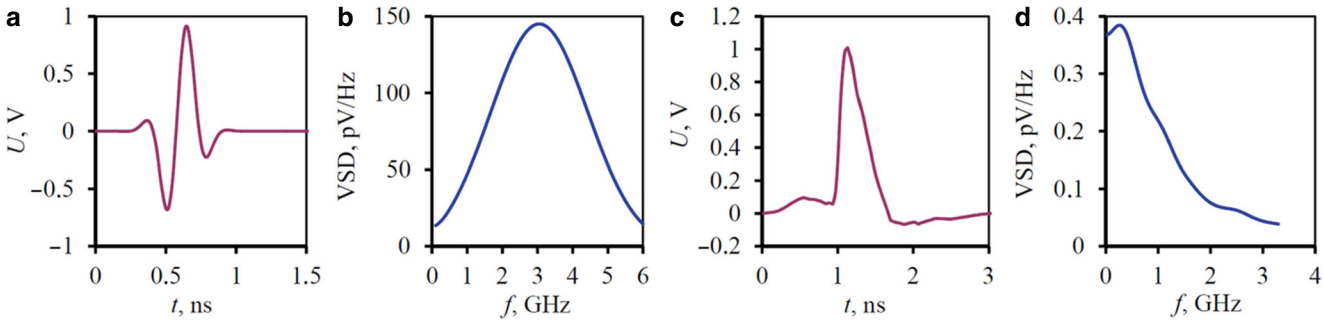


Fig. 9 Input excitation signals: Gaussian pulse **a** waveform and **b** spectrum, UWB pulse **c** waveform and **d** spectrum

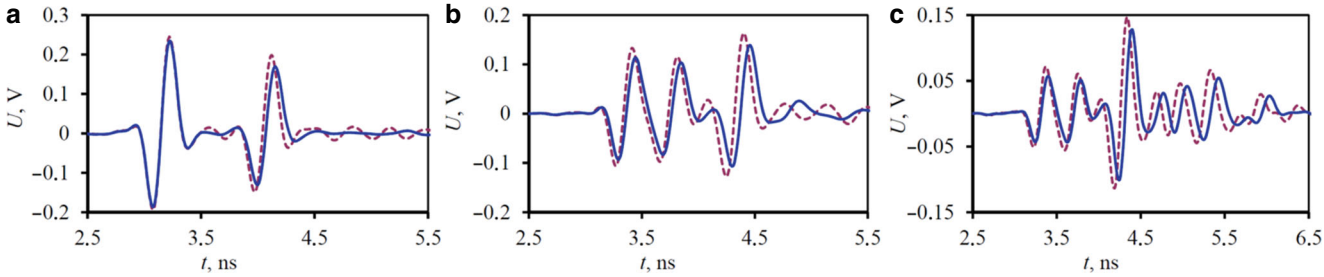


Fig. 10 Output responses to the Gaussian pulse: **a** LPF_1, **b** LPF_2, **c** LPF_3. Solid and dashed lines indicate measurement and simulation results, respectively

Figure 10 presents the voltage waveform and spectral density (VSD) at the prototype output under the Gaussian excitation. In the case of LPF_1, the input pulse is decomposed into two main pulses (even and odd modes) with the peak amplitude of 224 and 167 mV. In the case of LPF_2, the response consists of four pulses with the amplitude not exceeding 139 mV. In the case of the LPF_3, the response is further fragmented into eight pulses due to additional reflections from T-resonators. The maximum amplitude drops to 128 mV. The attenuation factor, defined as the ratio between the input and output peak voltages, grows from 3.25 for LPF_1 to 4.6 for LPF_2 and 6.2 for LPF_3. This confirms that T-resonators effectively redistribute the pulse energy over a longer time interval.

As shown in Fig. 11, the decomposition effect is even more pronounced for the shorter (300 ps) UWB pulse. Specifically, LPF_1 decomposes the input pulse into 2 components (191 and 153 mV), and LPF_2 generates a sequence of four pulses, reducing the peak voltage to 132 mV. The last structure produces a complex waveform of eight overlapping pulses with the peak level below 120 mV. In terms of the spectral density reduction, the average attenuation increases from 2.2 (LPF_1) to 3.65 times (LPF_3).

The results clearly demonstrate that the integration of T-resonators significantly enhanced the MF protective properties. While the frequency-domain analysis showed the moderate attenuation improvement (by ~6 dB), the time-domain analysis revealed the true physical mechanism, i.e., the multipath interference. T-resonators acted as delay lines that created additional signal paths. By optimizing their lengths, the reflected pulses were timed to arrive within the time intervals separating the primary even and odd mode pulses. This minimized the constructive interference (superposition) of the signal components, leading to a decrease in the instantaneous peak power of the interference without requiring a proportional increase in the physical length of the device.

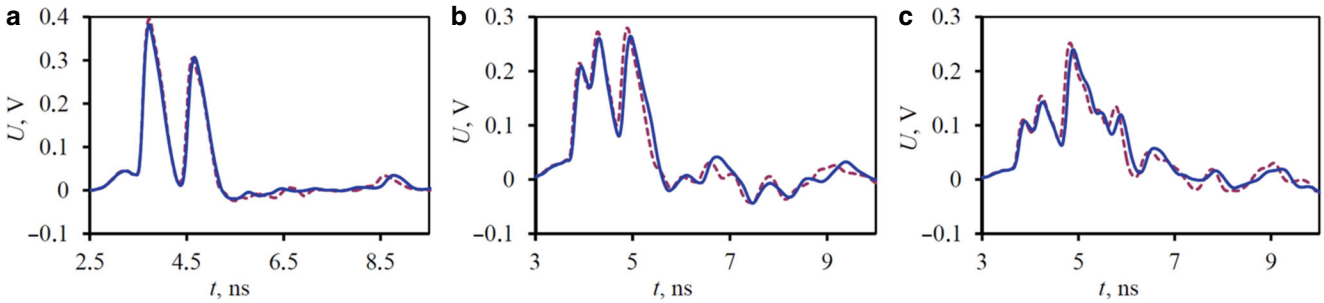


Fig. 11 Output responses to the UWB pulse: **a** LPF_1, **b** LPF_2, **c** LPF_3. Solid and dashed lines indicate simulation and measurement results, respectively

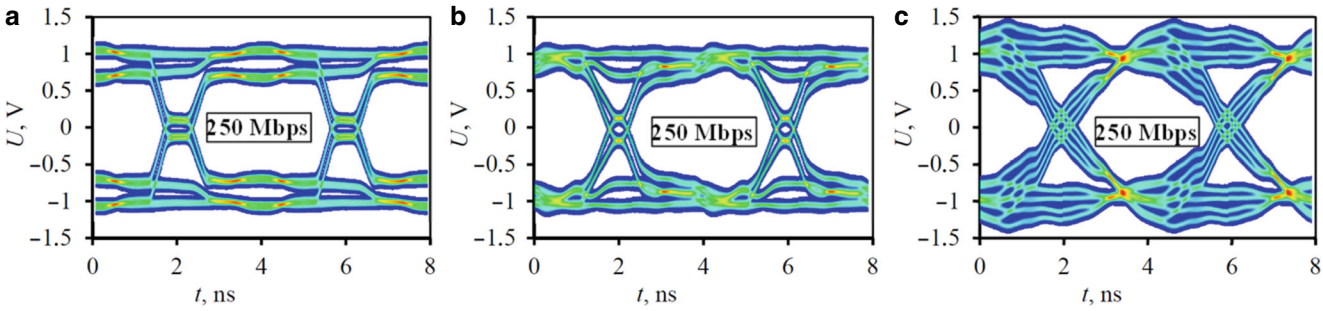


Fig. 12 Eye diagrams obtained for **a** LPF_1, **b** LPF_2, **c** LPF_3 at 250 Mbps data rate

Signal integrity analysis

Let us analyze the eye diagrams in Fig. 12 obtained for LPF_1, LPF_2, and LPF_3 to evaluate the impact of the proposed protective structures on the transmission of useful high-speed digital signals. A pseudo-random binary sequence with a length of 10^4 bits is used as the excitation source, and the structures are simulated at the data transmission rate of 125 and 250 Mbps and $0.1 \cdot T_{bit}$ (where T_{bit} is the bit duration) rise and fall time. Table 1 summarizes the quantitative parameters extracted from the diagrams (Eye Height, Eye Width, and Signal-to-Noise Ratio (SNR)).

Comparative analysis with state-of-the-art solutions

Let us compare the proposed hybrid structures within the current state of the art against analogous protection devices reported in [24–29]. The comparison metrics includes physical dimensions (area), cut-off frequency (f_c), insertion loss (IL), and return loss (RL) in both the passband (PB) and stopband (SB). The data are summarized in Table 2.

The proposed prototypes (LPF_1 and LPF_2) occupy a relatively large (4754 mm^2) area compared to compact microstrip filters (e.g., [29] with 319 mm^2). This is an inherent trade-off of the modal filtration technology. The length of the coupled section (l_m) determines the time difference ($\Delta\tau$) between modes and, consequently, the suppressed pulse duration. However, unlike lumped-element filters, the proposed structure is planar and can be integrated into the internal layers of a printed circuit board as part of the signal routing.

The most significant advantage of the investigated hybrid structures lies in their quasi-reflectionless behavior in the stopband. As shown in works [24] and [29], standard reflective filters provide the high (IL > 20 dB) attenuation, but extremely low RL in the stopband (RL ≈ 0.5 dB). This indicates that nearly 90–100% of the interference energy reflects back to the source, potentially damaging sensitive driver circuits. In contrast, LPF_3 demonstrates the mean return loss of 10.75 dB in the stopband. Although local resonant peaks of reflection (reaching –5 dB) occur near the transition band due to T-resonators, the integral energy absorption remains high across 0 to 18 GHz range. This confirms that the device functions mostly as a dissipative element, converting the interference energy into heat within the matching resistors, rather than reflecting it.

Table 1 Extracted Eye Diagram Parameters for 125 and 250 Mbps Data Rates

Bitrate (Mbps)	Structure	Eye height (V)	Eye width (ns)	JitterRMS (ps)	SNR
125	LPF_1	1.13	7.40	0.08	6.98
	LPF_2	1.12	7.52	0.05	7.20
	LPF_3	1.71	7.49	0.07	13.1
250	LPF_1	1.07	3.18	0.29	4.76
	LPF_2	1.16	3.33	0.21	9.15
	LPF_3	1.29	3.11	0.21	6.74

Table 2 Comparison of the Proposed Hybrid Structures with Analogous Solutions[1]

References	Area, mm^2	fc, GHz	PB		SB	
			Mean RL, dB	Mean IL, dB	Mean RL, dB	Mean IL, dB
LPF_1	61.5×64.2	0.17	16.7	1.83	11.70	17.9
LPF_2	71.5×66.5	0.19	18.1	1.63	11.66	21.6
LPF_3	71.5×66.5	0.15	12.4	1.32	10.75	24.3
[24]	229.6	0.87	25.6	0.30	1.20	25.3
[24]	590	1.00	19.3	0.40	0.50	23.2
[26]	27×13.7	0.82	10.2	0.90	2.00	38.5
[27]	40.4×23.4	0.90	15.5	0.50	3.20	29.4
[28]	2456.2	0.50	16.4	0.30	1.40	26.3
[29]	11×29	0.12	22.7	0.30	0.50	31.5

[1]RL values for the proposed structures represent the mean return loss averaged over the frequency range

It is important to note that dimensions and the frequency response of the proposed LPFs are scalable (depend on the size). For instance, reducing the MF length to 150 mm and scaling resonators accordingly, shift the cut-off frequency to ~560 MHz, making the device suitable for protecting against shorter pulses while significantly reducing the footprint.

Conclusions

This paper presented the comprehensive experimental study of electromagnetic wave propagation and interference in a hybrid protective structure based on broadside-coupled transmission lines and T-shaped resonators. The work focused on modal decomposition mechanisms and multipath interference as a means to suppress UWB pulses. Research findings can be summarized as follows.

– It was demonstrated that the integration of T-resonators into the MF structure significantly altered the time-domain response. Due to the additional signal paths created by the resonators, the input pulse was decomposed into a train of lower-amplitude pulses. For the 300 ps UWB pulses, the hybrid structure with two pairs of resonators reduced the peak voltage by 4.2 times. For the Gaussian pulse, the suppression factor reached 7.15. This confirmed that the proposed topology effectively redistributed the interference energy over time.
– Unlike conventional reflective filters, the proposed prototypes maintained the high return loss in the stopband. The measured mean return loss at 18 GHz, ranged between 10.8 and 11.7 dB, indicating that the interference energy did not reflect back to the source but was largely dissipated in matched terminations of the passive line, which was critical for the stability of sensitive radio-electronic systems.
– The introduction of resonant elements led to an increased group delay dispersion and phase non-linearities near the cut-off frequency. The eye diagram analysis showed that while these effects caused some inter-symbol interference, the "eye" remained open for 250 Mbps data rate, thereby providing a reliable transmission of useful digital signals.
– The comparative analysis showed that while the proposed structures occupied a larger area than lumped-element filters, they offered a unique combination of the high stopband absorption and planar integration capability. The design was scalable, allowing the cut-off frequency to be optimized for specific pulse durations.

In conclusion, the hybrid combination of modal filtration and T-shaped resonators proved to be a robust method for the UWB protection, offering a significant advantage in terms of the energy dissipation compared to standard reflective solutions.

Author Contribution All authors have contributed equally to the conception, design, data acquisition, analysis, interpretation, and writing the manuscript. All authors have read and agreed to the published version of the manuscript.

Funding This work was financially supported by Grant No. 24-79-00159 from the Russian Science Foundation.

Data availability The authors confirm that all data generated or analyzed during this study are included in this published article.

Declarations

Conflict of interest The authors declare no conflict of interest.

References

1. Usychenko, V.G., Sorokin, L.N., Sasunkevich, A.A.: Dependence of reversible and irreversible failures of semiconductor devices on the repetition rate of powerful pulse electromagnetic interferences. Radiotehnika i èlektronika **68**(12), 1450–1457 (2023). https://doi.org/10.31857/S0033849423120197
2. Gizatullin, Z.M., Gizatullin, R.M., Nuriev, M.G.: Methodology and models for physical simulation of electromagnetic interference using the example of analysis of noise immunity of electronic vehicle equipment. Radiotehnika i èlektronika **66**(6), 609–613 (2021). https://doi.org/10.31857/S0033849421060103
3. Bekkiev, A.Y., Borisov, V.I.: Assessment of noise immunity of radio communication channels under interference from electronic warfare means. J. Commun. Technol. Electron **64**(9), 891–901 (2019). https://doi.org/10.1134/S0033849419080003
4. Stepovik, A.P., Shamaev, E.Y., Armanov, M.M.: Influence of internal microcircuit traces on susceptibility to ultrashort pulses of ultra-wideband radiation. J. Radio Eng. Electron **62**(8), 812–818 (2017). https://doi.org/10.7868/S0033849417080137
5. Stepovik, A.P., Shamaev, E.Y., Khmelnitsky, D.V., Armanov, M.M., Kondratiev, A.A., Sorokin, I.A., Zavolokov, E.V.: Functional malfunction of a microcontroller under irradiation by bursts of ultrashort pulses of ultra-wideband radiation. J. Radio Eng. Electron **63**(3), 286–291 (2018). https://doi.org/10.7868/S0033849418030105
6. Meshcheryakov, S.A.: On the equivalence of exposure to high-power microwave pulses and video pulses of different polarities on semiconductor diode structures. J. Radio Eng. Electron **59**(2), 184–189 (2014). https://doi.org/10.7868/S0033849414010094
7. Radonić, V., Crnojević-Bengin, V.: Super-compact stopband filter based on grounded patch resonator. Electron. Lett **46**(2), 146–147 (2010). https://doi.org/10.1049/el.2010.3081
8. Zakharov, A.V., Ilchenko, M.E., Trubarov, I.V.: Planar three-resonator bandpass filters with cross coupling. J. Radio Eng. Electron **62**(2), 187–195 (2017). https://doi.org/10.7868/S0033849417020139
9. Gazizov, T.R., Zabolotsky, A.M.: New approach to EMC protection. In: Proc. 18th Int. Zurich Symp. on Electromagnetic Compatibility. Zurich, Switzerland (2007), pp. 273–276
10. Samoilichenko, M.A., Zhechev, E.S., Gazizov, T.R.: Experimental study of electrical characteristics of a modal filter on a double-sided printed circuit board. Radiotehnika i èlektronika **68**(11), 1131–1139 (2023). https://doi.org/10.31857/S0033849423070094
11. Belousov, A.O.: Cascading of three-conductor modal filters based on asymmetric coaxial structures and the microstrip line. Radiotehnika i èlektronika **68**(5), 601–608 (2023). https://doi.org/10.31857/S0033849423050029
12. Kosteletsky, V.P., Zabolotsky, A.M., Lakoza, A.M.: Two-cascade shielded modal filter for differential and common mode operation. Proc. Sci. Conf. "Development Problems of Prospective Micro- and Nanoelectronic Systtems" (2021). https://doi.org/10.31114/2078-7707-2021-4-127-133
13. Gazizov, A.T., Zabolotsky, A.M., Gazizov, T.R.: Decomposition of ultrashort pulse in structures with facial feedback. Russ. Phys. J **60**(3), 70–77 (2017)
14. Trubcheninov, V.A., Vlasov, S.V., Zhechev, E.S., Zabolotsky, A.M.: Method of layout of electromagnetic absorbers in the structures of small-size modal filters. JRE (2024). https://doi.org/10.30898/1684-1719.2024.10.14
15. Vlasov, S.V., Zhechev, E.S., Zabolotsky, A.M.: Analysis of characteristics of reflection-symmetric strip structure in differential mode. JRE (2025). https://doi.org/10.30898/1684-1719.2025.1.3
16. Samotin, I.E., Zabolotsky, A.M., Gazizov, T.R., Kirichek, R.V.: Use of a flat power cable as a protective device against ultrashort pulses. Dokl. Tomsk. Gosud. Univ. Sist. Upravl. Radioelektron **1**(21), 74–79 (2010)
17. Kosteletsky, V.P.: Review of hybrid filters for electronic equipment protection from conducted emissions. Dokl. Tomsk. Gosud. Univ. Sist. Upravl. Radioelektron **25**(1), 37–47 (2022). https://doi.org/10.21293/1818-0442-2021-25-1-37-47
18. Zhechev, Y.S., Adnan, A.H., Malygin, K.P.: New technique for improving modal filter performance by using an electromagnetic absorber. IEEE Access **10**, 86663–86670 (2022). https://doi.org/10.1109/ACCESS.2022.3199360

19. Zhechev, Y., Zabolotsky, A.: The use of quarter-wave resonators to improve modal filters performance. Proc. IEEE 22nd Int. Conf. of Young Professionals Electron Devices Mater. (EDM), the Altai Republic, Souzga (2021). https://doi.org/10.1109/EDM52169.2021.9507692
20. Ivantsov, I.A., Kalashnikov, I.V., Zhechev, Y.S.: Resonators in modal filter as a resource for improving its characteristics. Proc. IEEE 24th Int. Conf. of Young Professionals Electron Devices Mater. (EDM), N.Y., USA (2023). https://doi.org/10.1109/EDM58354.2023.10225187
21. Kuksenko, S.P.: Preliminary results of TUSUR University project for design of spacecraft power distribution network: EMC simulation. IOP Conf. Ser.: Mater. Sci. Eng **560**(1), 012110 (2019). https://doi.org/10.1088/1757-899X/560/1/012110
22. IEEE Std. 1597.1-2022: "IEEE Standard for Validation of Computational Electromagnetics Computer Modeling and Simulations". IEEE, New York, USA (2022)
23. IEC/TR 61000-1-5: Electromagnetic Compatibility (EMC)—Part 1-5: High Power Electromagnetic (HPEM) Effects on Civil Systems. IEC, Geneva, Switzerland (2004)
24. Yahya, S.I., Zubir, F., Nkenyereye, L., Hafez, M.A., Nouri, L., Assaad, M., Jizat, N.M.: A lowpass-bandpass triplexer with a new microstrip configuration and compact size for 5G and energy harvesting applications. IEEE Access **12**, 60264–60275 (2024). https://doi.org/10.1109/ACCESS.2024.3393836
25. Hayati, M., Shama, F.: A compact lowpass filter with ultra wide stopband using stepped impedance resonator. IEEE Microw Wirel Technol Lett **26**(1), 269–274 (2017). https://doi.org/10.1109/LMWC.2010.2047457
26. Nisamol, T.A., Abdulla, P., Hamsakutty, V.: Highly selective planar microstrip lowpass filter using interdigital hairpin resonator (IHR). Proc. 2nd Int. Conf. Comput. Appl. Inf. Security (ICCAIS), N.Y., USA (2019). https://doi.org/10.1109/CAIS.2019.8769446
27. Chen, F.C., Li, R.S., Chu, Q.X.: Ultra-wide stopband low-pass filter using multiple transmission zeros. IEEE Access **5**, 6437–6443 (2017). https://doi.org/10.1109/ACCESS.2017.2693344
28. Velidi, V.K., Sanyal, S.: Sharp roll-off lowpass filter with wide stopband using stub-loaded coupled-line hairpin unit. IEEE Microw Wirel Technol Lett **21**(6), 301–303 (2011). https://doi.org/10.1109/LMWC.2011.2132120
29. Wang, Y., Yu, M., Ma, K.: Substrate integrated suspended slot line and its application to differential coupler. IEEE Trans Microw Theory Tech **68**(12), 5178–5189 (2020). https://doi.org/10.1109/TMTT.2020.3026012

Publisher's Note Springer Nature remains neutral with regard to jurisdictional claims in published maps and institutional affiliations.

Springer Nature or its licensor (e.g. a society or other partner) holds exclusive rights to this article under a publishing agreement with the author(s) or other rightsholder(s); author self-archiving of the accepted manuscript version of this article is solely governed by the terms of such publishing agreement and applicable law.

Authors and Affiliations

I. A. Ivantsov[1] · S. V. Vlasov[1] · Y. S. Zhechev[1] · R. S. Surovtsev[1]

✉ S. V. Vlasov
sergei.v.vlasov@tusur.ru

[1] Tomsk State University of Control Systems and Radioelectronics, Tomsk, Russian Federation